Shrinkage Behavior of Poly(ethylene terephthalate) for a New Cementitious–Shrinkable Polymer Material System

S. C. Dunn, A. D. Jefferson, R. J. Lark, B. Isaacs

Cardiff School of Engineering, Cardiff University, Cardiff CF24 3AA, United Kingdom

Received 12 March 2010; accepted 27 July 2010
DOI 10.1002/app.33109
Published online 23 December 2010 in Wiley Online Library (wileyonlinelibrary.com).

ABSTRACT: An investigation of the transient thermomechanical behavior of poly(ethylene terephthalate) (PET) is presented with respect to a new composite material system in which shrinkable PET tendons are incorporated into a cementitious matrix to provide a crack-closure mechanism. A series of parametric studies of the effects of the geometry, temperature, and soak time on the mechanical properties of the polymer are presented. In particular, this article focuses on the shrinkage behavior and the development of stresses under restrained shrinkage conditions. A one-dimensional numerical model, which is essentially a modification of Zener's standard linear solid model, is presented with the aim of simulating aspects of behavior of particular relevance to tendons within the composite material system. The model comprises a temperature-dependent dashpot and spring in parallel with a spring and thermal expansion element. The temperature-dependent functions are calibrated with the obtained data, and a final validation example that shows good accuracy in comparison with experimental data not used for the calibration is presented. © 2010 Wiley Periodicals, Inc. J Appl Polym Sci 120: 2516–2526, 2011

Key words: composites; glass transition; modeling; polymer rheology; thermal properties

INTRODUCTION

This article addresses the performance of shrinkable polymers in the context of a new composite material system in which shrinkable polymer tendons are incorporated into a cementitious matrix to provide a crack-closure system. The overall material system has been described previously[1] and has been given the name LatConX, which is the subject of a pending patent.[2]

This work, undertaken to prove the concept of the material system,[1] comprised a series of tests of small-scale cementitious beams with embedded, unbonded polymer tendons. In these tests, the specimens were cast, cured for a few days, and then loaded to induce cracking. The polymer tendons were then activated with heat, and the resulting restrained shrinkage of the tendons imparted compression to the cementitious material; this served to close any cracks that had formed and to enhance autogenous healing of cracks.

A further aspect of the proof-of-concept work[1] was the establishment of minimum criteria for the polymer tendons with respect to their effectiveness in the LatConX material system.[1] A series of preliminary experiments were carried out to find shrinkable polymer materials that satisfied the performance criteria; from these tests, it was found that a commercially available, semicrystalline poly(ethylene terephthalate) (PET; Shrink Tite, Aerovac, Keighley, West Yorkshire, UK) best met the criteria.[1] The chosen PET material is called a drawn polymer because of the manufacturing process of drawing, which gives rise to its shrinkable shape-memory-like behavior.

The development of the composite material system and methods for its design require a predictive model for the polymer tendons, and this contribution describes the work undertaken to understand the behavior of the polymer and the simple one-dimensional model developed for simulating its time-dependent and temperature-dependent mechanical behavior.

Previous experimental studies of the temperature-dependent shrinkage behavior of PET were carried out by Gupta et al.,[3] who investigated the effect of the draw ratio on axially oriented PET samples heated to a variety of discrete temperatures. Gupta et al. found that restrained stresses were generated around the glass-transition temperature (T_g), and they attributed this to the tendency of the extended molecules to adopt more coiled conformations near T_g.

A number of authors have used Eyring's equation[4] to represent viscous behavior in modified versions of Zener's standard linear solid (SLS) model[5] to

Correspondence to: A. D. Jefferson (jeffersonad@cardiff.ac.uk).

Contract grant sponsors: Royal Society of Engineering Brian Mercer Feasibility Award (2007–2008).

simulate various aspects of the temperature-dependent behavior of PET. Sherby et al.[6] and Wilding and Ward[7] used this approach to simulate creep behavior; Guiu and Pratt[8] and Sweeney and Ward[9] used it to simulate stress relaxation; and finally, Sweeney et al.[10] used it to simulate yield behavior.

A different approach, based on similar principles, was developed initially by Pakula and Trznadel[11] and subsequently by Morshedian et al.[12] Pakula and Trznadel proposed a four-state model to describe the temperature dependence of amorphous polymers. The model is characterized by two elastic springs and two two-site elements. This multisite element model simulates the local properties of a molecular subunit and its interactions with the matrix. Morshedian et al. replaced the two-site elements with temperature-dependent dashpots.

Bhattacharyya and Tobushi and coworkers[13] proposed a four-element rheological model comprising an elastic spring and a viscous dashpot in parallel with a friction element and a second viscous dashpot to simulate the isothermal mechanical behavior of polymers. It is the friction element that models the effect of shape-memory strain. Tobushi et al.[14] in a later article proposed that the material parameters (modulus of elasticity, viscosity, retardation time, and coefficient of thermal expansion) should be exponential functions of temperature.

Zener et al.'s SLS model,[5] although providing a good first approximation of the observed behavior of polymers in their viscoelastic range and describing both creep and stress relaxation, does not include the effects of temperature and shrinkage on the deformation behavior.

The overall aim of the work described in this article was to develop a one-dimensional constitutive model for the time-dependent behavior of shrinkable PET that could be used in the design of the LatConX material system. To develop such a model, the viscoelastic and shrinkage properties of the selected PET material were investigated in a series of experiments. These examined the effects of the heating rate and soak time (i.e., the time of a material's exposure to a certain constant temperature) on the elastic properties and shrinkage stress of PET samples. The specific polymer modeling requirements of the LatConX system are addressed in the following section.

LatConX CONCEPT

The LatConX system, illustrated in Figure 1, has embedded polymer tendons that are initiated once cracks have occurred in the cementitious material. Upon the identification of such cracking, the drawn polymer, which is anchored at discrete points, is activated via heating. This causes a tensile force to develop in the restrained tendons, which in turn

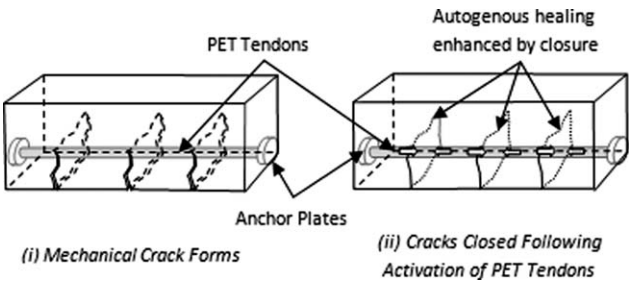

Figure 1 LatConX system.

impart a compressive force to the matrix and thereby close any open cracks. Autogenous healing then occurs and is enhanced by the cracks being put into this compressive state.[15] Studies aimed at further enhancing this autogenous healing have also been carried out, and these have demonstrated 85% strength recovery from autogenous healing.[16]

During heating and cooling, the cementitious matrix will undergo thermal expansion and contraction, but it will also shrink because of drying and residual hydration. After activation, the matrix will be subjected to continued drying shrinkage as well as long-term creep. Furthermore, the polymer tendons themselves will undergo relaxation after activation. Thus, the polymer model will need to be able to simulate relatively complex time-dependent thermomechanical behavior if it is to correctly predict the performance of the tendons within this material system.

EXPERIMENTAL

Material

The material used for the following experiments was selected in a pilot project that incorporated a material screening exercise.[1] The primary criterion used for material selection was that it should develop a restrained shrinkage stress of at least 20 MPa. Further selection criteria were that (1) the temperature of stress development should occur between 70 and 90°C to prevent premature activation during the hydration process of the cementitious material or damage to surrounding concrete, (2) the material should also be inert in an alkaline environment, and (3) the shrinkage stress that develops during activation should not decrease by more than 30% throughout the working life of the structure (50 years for buildings and 120 years for bridges). The screening tests highlighted Aerovac Shrink Tite, a drawn PET polymer material that is readily available in 32 mm $\times$ 0.046 mm tape form, as best suiting these criteria.[1]

Test specimen preparation

The tested specimens included a number of PET strips that were nominally 6-mm-wide (actual mean

Figure 2 Manufacturing process for the specimens.

width = 5.8 mm) and 450 mm long; these were formed into tendons by being laid in a specially designed jig, as shown in Figure 2. The strips were then bonded together with a soldering iron, which was used to melt the ends. The standard number of strips was 25, although specimens with more strips were used in one test series, which checked the dependence on geometrical parameters.

Two steel plates ($10 \times 20 \times 3$ mm^3) were then placed at either end of the 450-mm-long specimens at a distance of 360 mm, as shown in Figure 4, to form end anchors. The remaining length of the polymer was then melted, as shown in Figure 3, to create a mechanical plug, which served as a mechanical lock to prevent slippage. Figure 4 shows the form of the specimen before its placement in the grips of the testing machine. This anchor system was tested in a series of preliminary experiments in which slip at the grips was monitored locally. These tests showed

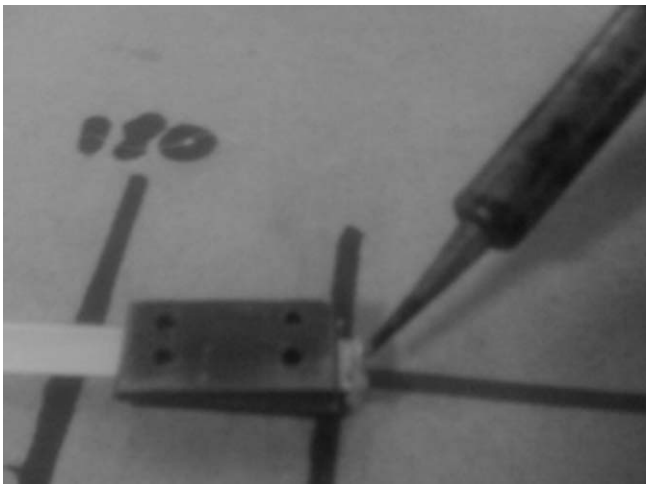

Figure 3 Creation of a mechanical plug.

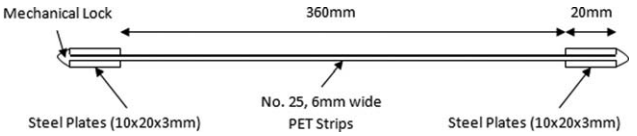

Figure 4 Specimen preparation.

that the final anchor system described here ensured no end slip.

Equipment

The experiments were undertaken with a Dartec tensile testing machine fitted with an Instron environmental chamber capable of temperatures ranging from −50 to +250°C. The experimental setup can be seen in Figure 5(a,b).

The specimen, with end plates attached, was placed between the machine grips, as shown in Figure 6, and a preload was applied to remove any slack. The chosen preload was equivalent to a prestress of 1.36 MPa.

Test series

A series of parametric studies were then undertaken in which the displacement at the grips, load, and environmental chamber temperature were continuously monitored. The maximum monitoring rate of the data logger (i.e., 100 readings/s) was used when the temperature or load rate was at a maximum, but lower sampling rates were used for other cases.

In all cases, unless otherwise noted, each test was undertaken three times. Thus, the quoted mean values are averages of three tests.

Geometric parameters

Sections of different cross sections and lengths were tested to assess the effects of geometric properties on the measured shrinkage stress. Sections containing 25 strips (6.9 mm^2), 50 strips (13.8 mm^2), and 75 strips (20.7 mm^2) were tested at a length of 350 mm, and specimens 360 or 180 mm long with 25 strips were also tested. Each specimen was held at a constant displacement while the temperature was raised to 90°C at a rate of 0.41°C/s; it was then soaked for 30 min before the temperature was reduced to the ambient temperature for 10 min

Study of stress development with temperature

A 360-mm-long specimen containing 25 strips (a standard specimen) was held at a constant displacement while the temperature was raised to 90°C at a rate of 0.41°C/s; it was soaked for 3 h before the

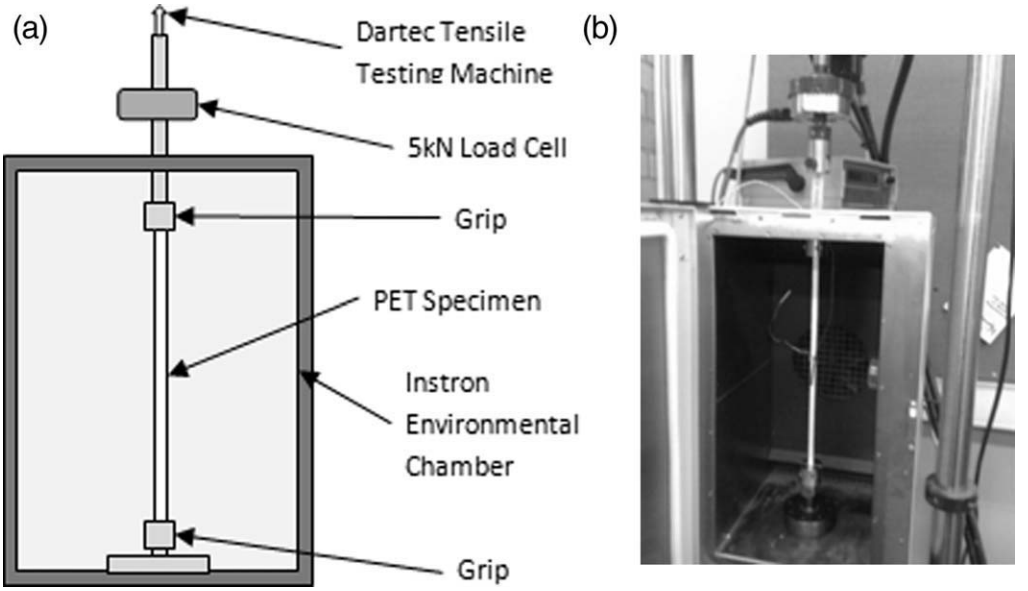

Figure 5 (a) Diagram of the equipment setup and (b) photograph of the material setup.

temperature was reduced to the ambient temperature for another hour.

Study of the effect of the soak time on stress development

A standard 360-mm specimen was held at a constant displacement while the temperature was increased in 10°C increments from 30 to 170°C. At each 10°C increment, the temperature was held for the chosen soak time. Three different soak times were investigated: 0 min, 5 min, and 1 h. Between each increment, the temperature was raised at a rate of 0.13°C/s.

Study of the effect of temperature on Young's modulus: the *E*-value test

A standard specimen was held at a constant load while the temperature was raised in 10°C increments from 30 to 160°C. At each temperature increment, the specimen was soaked for 5 min, and then a loading/unloading cycle with an amplitude of 10 N was applied at a specified rate. Three rates were used: 10, 1, and 0.1 N/s. This loading–unloading cycle is called the *E*-value test, and it was repeated for every temperature increment.

Study of the free shrinkage development with temperature

Throughout the Young's modulus study, the displacement of the specimen was recorded, and this enabled the shrinkage–temperature relationship to be studied.

RESULTS AND DISCUSSION

The results for each of the aforementioned test series are considered in the following.

Study of the geometric parameters

Figure 7 shows the stress development for the 360-mm-long specimens with three different cross-sectional areas. This indicates that the effect of various cross-sectional areas on stress development is limited (maximum = 4%) in the range considered. Nevertheless, we expect that the greater the cross-sectional area is, the greater the temperature difference will be between the surface and the center of the cross section. To explore whether this temperature lag is responsible for the aforementioned differences, a two-dimensional finite-element transient

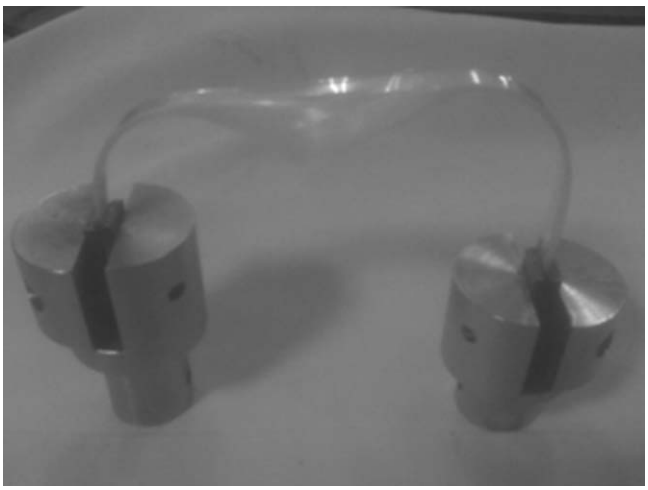

Figure 6 Photograph of the grip setup.

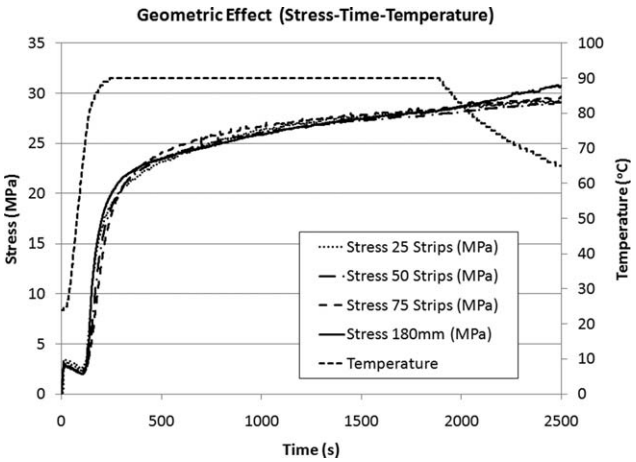

Figure 7 Response for different geometries.

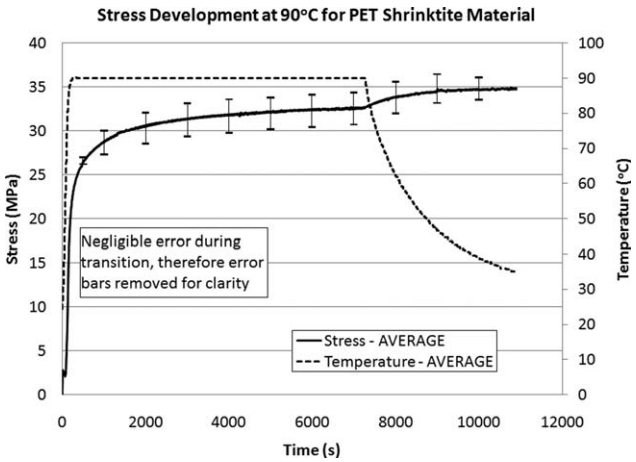

Figure 9 Stress development with time.

thermal analysis was undertaken for each of the cross sections. The results for the three cross sections are shown in Figure 8 in terms of the center-of-specimen temperature versus time. These results provide justification for the slightly differing stress paths during the early stages of stress development. The thermal analysis highlights that after 930 s (15.5 min), full temperature saturation is achieved for all three cross-sectional areas. Figure 7 also highlights that a shrinkage stress of 29 MPa can be generated during a 30-min soak time, which exceeds the 20-MPa criterion set for the LatConX system.

There is a noticeable difference in shrinkage stress between the 360- and 180-mm specimens in the cooling phase at the top of the graph in Figure 7. The difference, which rises to 2 MPa, can be attributed to the thermal contraction of the 180-mm aluminum extension arm required for the shorter specimen. The calculated contraction of the arm for cooling from 90 to 64°C is 0.108 mm; with the measured Young's modulus of the polymer, this equates to a stress change in the polymer of 2.1 MPa.

Stress development with temperature (Figs. 9 and 10)

Figures 9 and 10 show stress development with time and temperature, respectively. The shrinkage stress is generated at a decreasing rate and reaches a plateau at approximately 32.5 MPa after a 3-h soak at 90°C; this is consistent with the magnitude of the shrinkage stress found in the literature.[11] The generation of shrinkage stresses is a well-known property of drawn polymers and is associated with the orientation of the long-chain molecules in the direction of drawing.[17,18] Trznadel and Kryszewski[17] suggested that the shrinkage-stress potential of partially extended polymer chains is associated with the "entropic tendency of the chains to assume more coiled conformations." The stress plateau is consistent with the findings of Gupta et al.,[3] who suggested that the increase in crystallization occurring above T_g stabilizes the oriented state and reduces the relaxation potential, which is seen in the plateau of the shrinkage-stress response.[17]

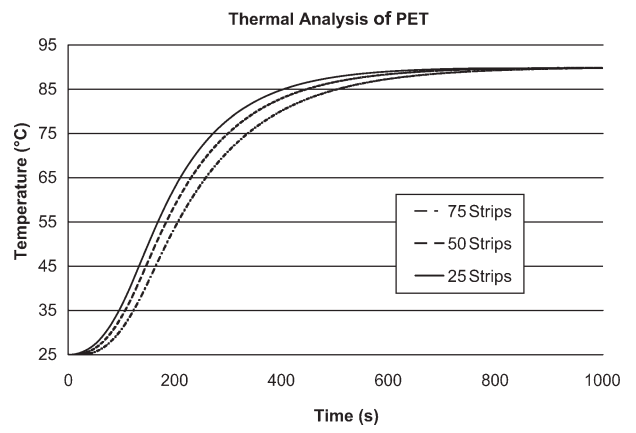

Figure 8 Results from thermal analysis.

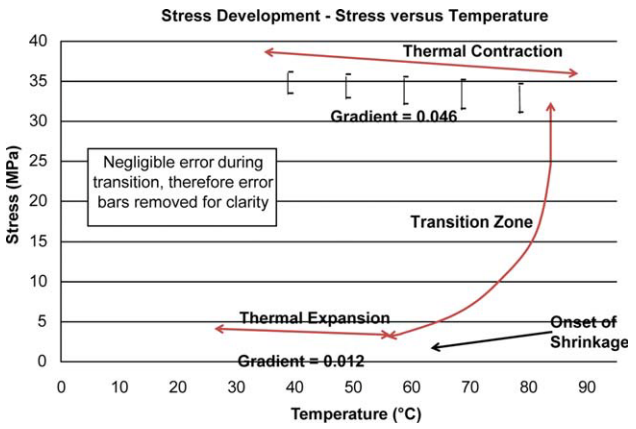

Figure 10 Stress development with temperature with highlighted regions.

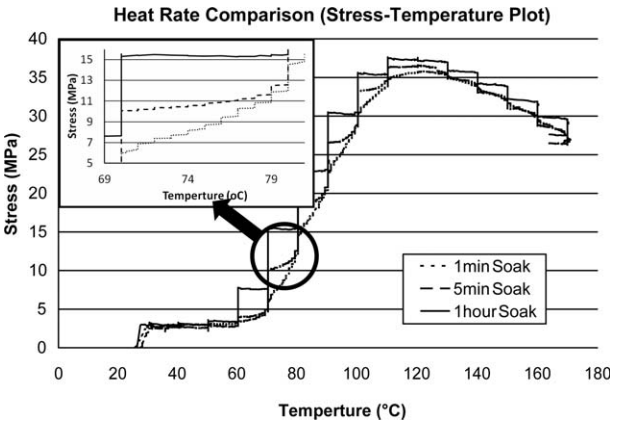

Figure 11 Comparison of the soak time experiments (stress–temperature plots).

The stress rise at the end of the test can be attributed to thermal contraction of the polymer upon cooling. Trznadel and Kryszewski[17] explained that the shrinkage that has occurred previously, which is associated with molecular coiling, is permanent and unrecoverable, but the independent molecular action of thermal expansion is recoverable.[17]

It has been found by others[17,19] that annealing (heating above the transition temperature) slightly increases the coefficient of thermal expansion, and this provides an explanation for the difference between the below-T_g expansion and contraction slopes at the start and end of the graph, respectively.

Three distinct regions can be seen in Figure 10: an initial thermal expansion zone, a transition zone, and a final thermal contraction region upon the removal of heat. The initial decrease in stress can be attributed to the thermal expansion of the polymer in the pre-shrinkage stage, which, under these constant strain–displacement conditions, gives rise to this decrease in stress. As the transition zone is reached, shrinkage becomes the dominant process, and thermal expansion becomes negligible.[17] The onset of shrinkage occurs between 60 and 70°C, and this is consistent with published values of T_g for PET.[3,18]

The calculated maximum stress that develops is a function of the cross-sectional area. The measured mean and standard deviation of the strip widths are 5.77 and 0.16 mm, respectively. A change in width equal to the standard deviation would equate to a calculated stress change of approximately 0.8 MPa for an individual strip.

Effect of the soak time on stress development (Figs. 11 and 12)

Figure 11 presents trends of the average stress versus temperature for the three investigated soak times; the averages are based on three tests per soak time. The graph shows that the maximum stress is achieved at 120°C, after which the stress decreases. This approximately matches the recrystallization temperature identified by Jog.[20] Gupta et al.[3] also highlighted that above 100°C, a large increase in the crystallinity occurs. It is known that this recrystallization process affects the potential for shrinkage to occur because when part of a molecular chain is incorporated into a crystallite, during recrystallization, the stress exerted at the molecule ends is reduced.[3,17]

If it is assumed that T_g is associated with the onset of shrinkage, Figure 12 suggests a T_g value of 70°C, which is consistent with previous observations by Gupta et al.[3] and Ward and Sweeney.[18]

The exploded view of the 70–80°C transition in Figure 11 shows that the stress for the 1-h soak time actually decreases throughout the temperature transition, whereas for the two shorter soak times, the stress consistently increases. It appears that two competing mechanisms are occurring at different rates: stress relaxation and shrinkage. The shrinkage is a relatively fast mechanism that stabilizes in approximately 5 min, whereas stress relaxation is slower and becomes apparent only during the 1-h soak time tests.

The peak stresses are 35.5 (1-min soak), 36.5 (5-min soak), and 37 MPa (1-h soak), and this suggests that a soak time of 5 min is sufficient. The increase in stress between temperature increments remains relatively small until the temperature of 70°C is reached. In the region of 70–90°C, that is, the glass-transition region,[14] the stress increases by approximately 7.5 MPa per 10°C increment. In all cases, the peak stress is reached at approximately 120°C, beyond which the stress decreases at approximately the same normalized rate.

Effect of the temperature on Young's modulus: the *E*-value test (Figs. 13 and 14)

The average response of the specimens during the *E*-value test was not independent of the continuing

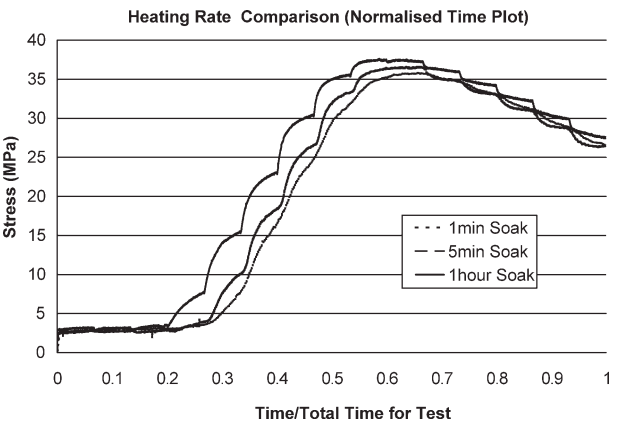

Figure 12 Normalized time plot.

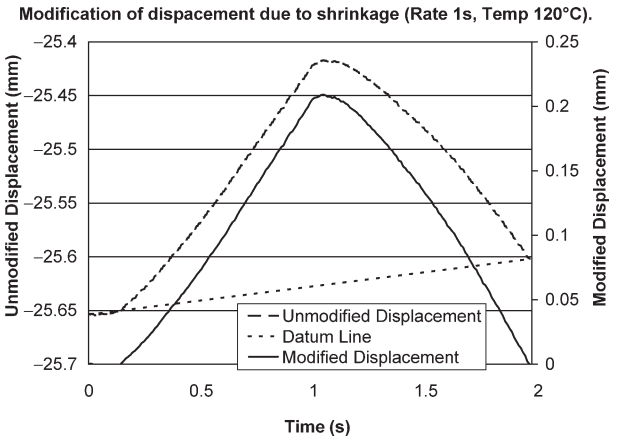

Figure 13 Modification of displacement due to ongoing shrinkage.

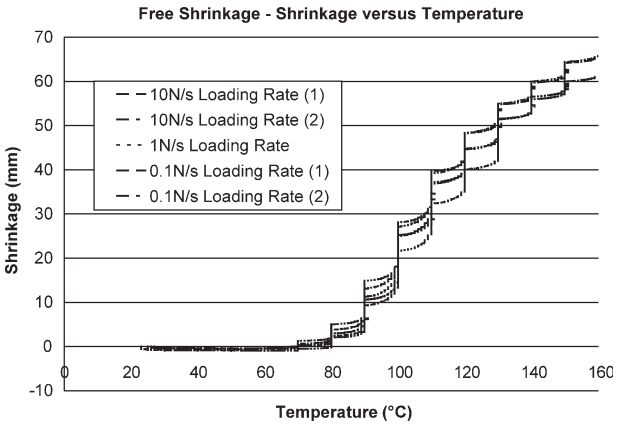

Figure 15 Free shrinkage versus temperature.

overall shrinkage, with the response during lower loading rate cycles being more affected by overall shrinkage than the response during the higher loading rate cycles. To allow for this, we applied a correction, as illustrated in Figure 13, in which a modified response was obtained by the consideration of the displacement with respect to the overall shrinkage trend line. The overall shrinkage displacement (or trend line) was assumed to vary linearly with time over the duration of the *E*-value test, as illustrated in Figure 13. The difference between the shrinkage trend line and unmodified displacements over a given time interval is termed the modified displacement.

These modified responses were used to calculate apparent Young's moduli; the results are shown in Figure 14.

The results from the tests at the three different loading rates (0.1, 1, and 10 N/s) agree with the work of Tobushi et al.[14] It can be concluded that apparent Young's moduli are relatively constant before the glass-transition region, decrease throughout the transition region, and become constant again after the transition region. The experiments presented in Figure 14 show that the slower rates have a lower apparent Young's modulus at a given temperature, and this highlights some rate dependence. The reduction in apparent Young's moduli with a decreasing loading rates is assumed to be due to viscous relaxation, which increases with decreasing loading rates.

It is known that Young's modulus decreases with increasing crystallization,[21] and it is also known that the amount of crystallization increases with time in the transition temperature range.[20] Thus, the observed rate dependence of the apparent Young's modulus is explained by different degrees of crystallization.

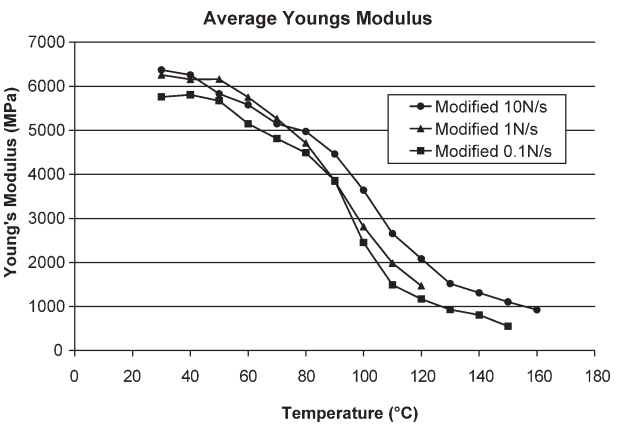

Figure 14 Young's modulus versus temperature.

Free shrinkage development with temperature (Fig. 15)

Plots of shrinkage versus temperature for each of the experiments mentioned in the previous section are shown in Figure 15. The experiments were continued only up to 160°C because at this temperature the testing machine reached maximum travel on account of the high levels of shrinkage exhibited by the specimens. The total shrinkage strain achieved at the end of the tests was 18.1%.

CONSTITUTIVE MODEL

Introduction

A constitutive model, based on Zener's SLS model[5] and modified with temperature-dependent springs and dashpots, was developed. Trznadel and Kryszewski[17] reported that the "construction of molecular models is extremely difficult" and that their analytical solution is "impossible". Therefore, as Trznadel and Kryszewski suggested, a phenomenological model is more appropriate, and the following

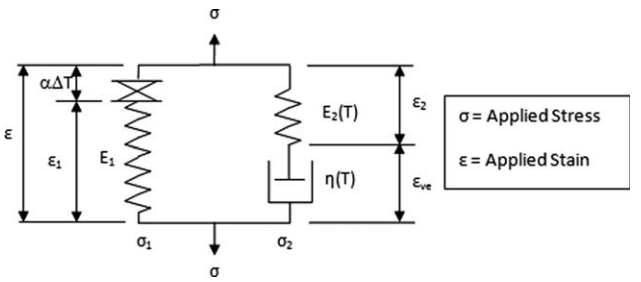

Figure 16 Rheological representation of the proposed model.

describes a proposed phenomenological representation for PET.

The relationship between Young's modulus and temperature is based on the observations of Tobushi et al.[14] and the experimental data presented in this article. The model is designed to simulate the transient thermomechanical behavior of PET in a one-dimensional uniaxial form.

Proposed constitutive model

The rheological model comprises an elastic spring (E_1) in parallel with a temperature-dependent elastic spring (E_2) and a temperature-dependent viscous dashpot (η) as shown in Figure 16.

The total stress (σ) is calculated as follows:

$$\sigma = \sigma_1 + \sigma_2 \tag{1}$$

The stress component in each arm of the model is determined as follows:

$$\sigma_1 = E_1.\varepsilon_1 \tag{2a}$$

$$\sigma_2 = E_2(T).\varepsilon_2 = \eta.\dot{\varepsilon}_{ve} \tag{2b}$$

where η is the viscosity and ε_{ve} is the viscoelastic strain. The solution to eqs. (1) and (2) is relatively standard:[22]

$$\varepsilon_{ve} = \int_{t_0}^{t} \frac{1}{\tau}.e^{-t-s/\tau}.\varepsilon(s)ds \tag{3}$$

where t is the time in which s is time variable, t_0 is the initial time, and $\tau = \eta/E_2$ is the relaxation-time parameter.

If the integration is considered over the time interval of t to $t + \Delta t$ and if the strain (ε) is taken as a constant within the interval with a value of ε_θ at time $t + \theta\Delta t$, where θ is a time interval parameter ($0 \leq \theta \leq 1$), then the viscoelastic strain at time t_j (ε_{ve_j}) in terms of its value at time t_{j-1} ($\varepsilon_{ve_{j-1}}$) is given by calculated as follows:

$$\varepsilon_{ve_j} = \varepsilon_{\theta_j}\left(1 - e^{-\Delta t/\tau}\right) + \varepsilon_{ve_{j-1}}.e^{-\Delta t/\tau} \tag{4}$$

where Δt is equal to $t_j - t_{j-1}$ and θ is taken to be 0.5.

The characteristic forms of the temperature dependence of both η and Young's modulus at the high temperature (E_{TOT}) are shown in Figure 17 and can be derived from experimental data, as explained later. E_{TOT} is the instantaneous value of $E_1 + E_2$, and the transition zone may be captured with the same form of function:

$$\eta(T) = \eta_L + (\eta_H - \eta_L)\frac{e^{a\chi(T)}}{e^{a\chi}(T) + b} \quad if\ T > T_L \tag{5a}$$

$$\eta(T) = \eta_R \quad if\ T \leq T_L \tag{5b}$$

$$E_{TOT}(T) = E_1 + (E_{TL} - E_1)\frac{e^{c\chi(T)}}{e^{c\chi(T)} + d} \tag{6}$$

where

$$\chi(T) = \frac{T - T_g}{T_H - T_L}$$

η_L is the viscosity at the low-temperature limit, η_H is the viscosity at the upper-temperature limit, b and d are elastic modulus material parameters, a and c are the viscous material parameters, T is the current temperature, T_g is the temperature at the center of the transition region, T_H is the high temperature above which the parameter is constant, and T_L is the low temperature at which the parameter is constant before the transition. The material parameters (a, b, c, and d) can be deduced from experiments and are presented later.

The aforementioned functions have been simplified from tanh functions.

At lower temperatures, the viscosity jumps to a much higher value (η_R),[12] and this governs the long-term relaxation, as shown in Figure 17.

The measured viscosity values from the experiments were used to evaluate η_H and η_L, as shown on Figure 17. A direct method for calibrating the constants in the viscosity function from experimental data is described later.

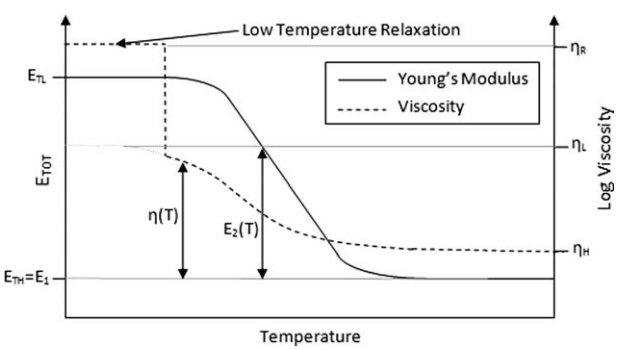

Figure 17 Generalized representation of η and E_{TOT} versus the temperature.

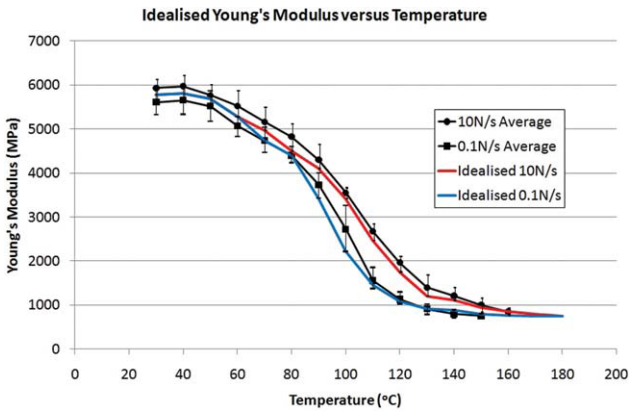

Figure 18 Plot of Young's modulus versus the temperature showing idealized values for viscosity calculations. [Color figure can be viewed in the online issue, which is available at wileyonlinelibrary.com.]

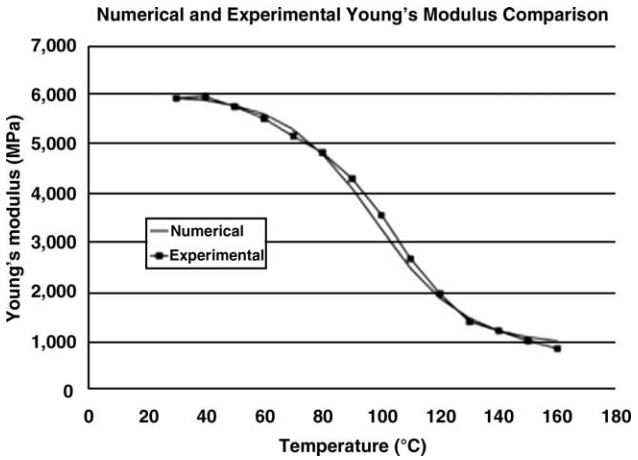

Figure 19 Stress–temperature response.

It is assumed that the value of E_1 is equal to the total short-term Young's modulus at the high temperature (E_{TH}).

The stress at time increment j (σ_j) may be obtained from eqs. (1), (2a), and (2b), and if thermal expansion is also allowed in arm 1, this stress is given by

$$\sigma_j = E_1[\varepsilon_j - \alpha_T(T_j - T_0)] + E_2(T).(\varepsilon_j - \varepsilon_{ve_j}) \qquad (7)$$

where ε_j is the strain at time increment j; T_0 is the ambient temperature; T_j is the temperature at time t_j and α_T is the coefficient of thermal expansion, which is known to have a significant effect on the total strain before the onset of shrinkage.[17]

Calibration of the material constants

For reasonable calibration of material constants, the experimental data need to be interpreted in light of the following model assumptions:

1. The apparent Young's modulus is independent of the temperatures below and above the transition range.
2. The difference between the apparent Young's moduli from the fast and slow loading rate tests is due to the temperature-dependent viscosity in the transition range.
3. Relaxation from viscosity is insignificant at the fastest loading rate used (i.e., 10 N/s).
4. Short-term relaxation is complete by the end of each step in the 0.1 N/s tests.

Figure 18 presents the data from Figure 14 with error bars for the 0.1 and 10 N/s loading rates and shows the associated lines best fitting the original data that comply with the aforementioned assumptions. We think that the data do reasonably support the assumptions, but we equally acknowledge that other mechanisms for which we have not accounted are in operation. It is also noted that these assumptions are consistent with those of Tobushi et al.[14] and Morshedian et al.[12] and are further supported by the good matches between the results from the predictive analyses and the experimental data presented in Figures 19 and 20. These idealized E-value data were used to calculate the parameters.

The 10 N/s E-value tests were used to calculate the material parameters for the E_2 function [eq. (6)] because the viscous strain rate is considered negligible at this loading rate. From the experimental data, the value for E_1 was assumed to be equal to the value of E_{TH}, as shown in Figure 17.

To determine the value of the viscosity for a range of temperatures, an inverse parameter identification exercise was undertaken with the apparent Young's modulus, as defined in eq. (8) and shown in Figure 18. Data from the low loading rate tests were used

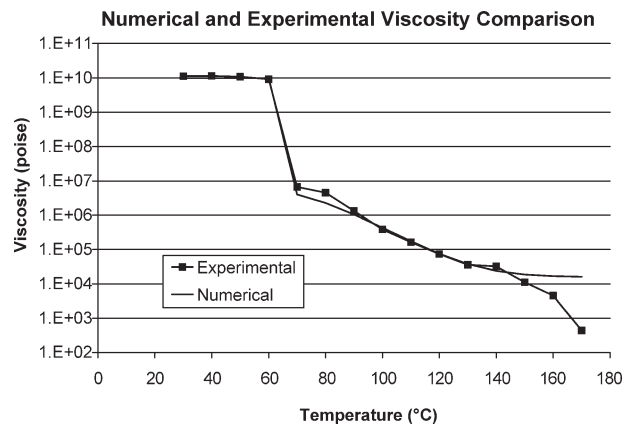

Figure 20 Stress–time response.

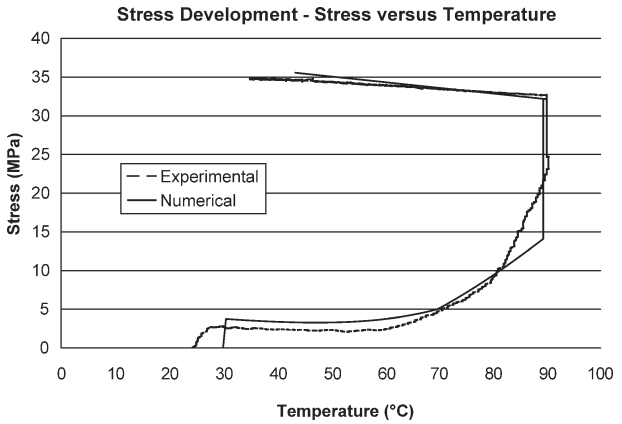

Figure 21 Comparison of numerical and experimental Young's modulus values.

(i.e., 0.1 N/s) because at this rate, the viscous response is known to be significant:

$$\text{Apparent Young's modulus } (E_{\text{app}}) = \frac{\Delta\sigma}{\Delta\varepsilon} \qquad (8)$$

Equation (8) was then used in eq. (1) and rearranged to determine the change in the viscous strain:

$$\Delta\varepsilon_{ve} = \Delta\varepsilon\left(1 - \frac{E_{\text{app}} - E_1}{E_2(T)}\right) \qquad (9)$$

If it is assumed that full relaxation has taken place before the start of a stress excursion (at time t) in an E-value cycle, such that ε at time t is equal to ε_{ve} at time t, then η may be derived from eqs. (3), (7), and (9) as follows:

$$\eta = \frac{-\Delta t.E_2}{ln\left((1 - \frac{1}{\theta}) + \frac{(E_{\text{app}} - E_1)}{E_2(T)}\right)} \qquad (10)$$

where θ is taken to be 0.9.

It can be seen from Figures 19 and 20 that the calibrated expressions for E_{TOT} and η closely match the experimental data from which they were derived. They are also consistent with the work of Tobushi et al.[14] (Young's modulus) and Morshedian et al.[12] (viscosity). The differences between the matched and experimental Young's moduli are considered inconsequential, but other workers have noted a high degree of variation in measured values for Young's modulus.[23]

The sharp drop in the viscosity before the transition zone is consistent with the model assumptions and is associated with the release of locked-in stress.[12] The difference between the derived and experimental viscosities beyond 140°C is partly attributable to the onset of melting and partly to the growth of the crystalline phase at these temperatures; neither is addressed in this model.[3,12]

Model assumptions

The previous sections describe the individual components of the model. Here, the underlying assumptions are summarized for convenience:

- The material behaves in a viscoelastic manner
- Temperature-dependent behavior can be simulated with a modified SLS model in which the viscous dashpot and the linked elastic component are temperature-dependent functions.
- The temperature-dependent elastic component and the viscosity can be reasonably represented with a modified tanh function.
- The high-temperature response can be used to derive the invariant elastic component.
- Below T_g, the viscosity is assumed to be a value associated with long-term relaxation of the polymer at the ambient temperature.

The model is considered to be generally suitable for simulating the transient thermomechanical behavior of drawn semicrystalline polymers below melting, and its applicability is not restricted to the specific material considered in this article.

Model validation

Table I presents the material parameters established in the previous calibrations.

A model validation example is now considered with an experiment not used in the calibration process. This consisted of heating a 360 × 6 × 2.3 mm^3 polymer sample to 90°C at a constant rate and then maintaining the temperature at 90°C for 3 h while the stress was monitored. Figures 21 and 22 show that good agreement is achieved between the numerical and experimental results for both temperature and time representations. There is, however, a

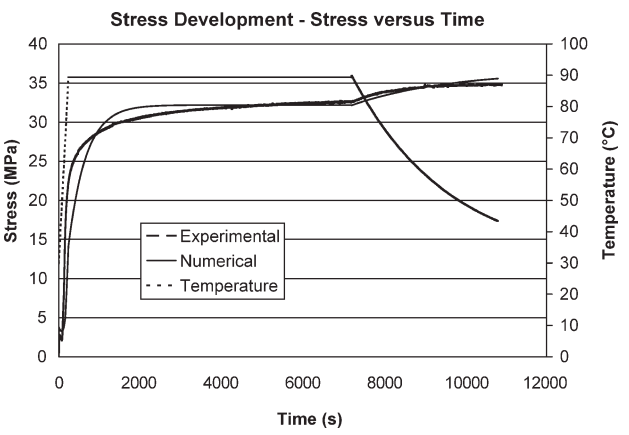

Figure 22 Comparison of numerical and experimental viscosity values.

TABLE I
Numerical Input Values

Name	Symbol	Value
Ambient temperature	T_0	30°C
Coefficient of thermal expansion	α_T	$10^{-4.1}$
Young's modulus at the low temperature	E_1	845 MPa
Young's modulus at the high temperature	E_{TOT}	6000 MPa
Transition start temperature (Young's modulus)	T_L	70°C
Transition end temperature (Young's modulus)	T_H	120°C
Temperature at the center of the transition (Young's modulus)	T_g	95°C
Elastic modulus material parameter	b	3.3
Elastic modulus material parameter	d	1.2
Stress at drawing	σ_{res}	36 MPa
Viscosity at high temperatures	η_{2L}	1.575×10^4 P
Viscosity at low temperatures	η_{2H}	7.322×10^7 P
Transition start temperature (viscosity)	T_L	30°C
Transition end temperature (viscosity)	T_H	110°C
Temperature at the center of the transition (viscosity)	T_g	70°C
Viscous material parameter	c	5
Viscous material parameter	f	0.1

noticeable difference between the numerical and experimental responses in Figure 22 that can be attributed to the fact that the temperature in the specimen lagged behind that of the thermocouple in the oven used in the presentation of the data.

CONCLUSIONS

A detailed study of the shrinkage behavior of PET has been presented along with a numerical model for predicting the transient thermomechanical behavior in one dimension. The studies have been carried out as part of the development of a new material system called LatConX.

T_g for the tested PET is approximately 70°C. The variation of Young's modulus with temperature follows a modified tanh function as proposed by Tobushi et al.[14] The viscosity also varies with temperature according to a tanh-type function after activation from a near solid condition, as proposed by Morshedian et al.[12]

The obtained results were effectively independent of the geometry of the specimens once a temperature lag correction had been applied. The peak shrinkage stress was achieved at 90°C with a soak time of 15 min.

The proposed one-dimensional, temperature-dependent viscoelastic model can accurately predict the transient shrinkage response of drawn PET from room temperature to the onset of melting.

The authors thank Ian Ward and John Sweeney for their comments on certain aspects of this work.

References

1. Jefferson, A. D.; Joseph, C.; Lark, R. J.; Isaacs, B.; Dunn, S. C.; Weager, B. Cem Concr Res 2010, 40, 795.
2. Jefferson, A. D.; Lark, R. J.; Joseph, C. Brit. Pat. GB0715123 (2007).
3. Gupta, V. B.; Radhakrishnan, J.; Sett, S. K. Polymer 1994, 35, 2560.
4. Halsey, G.; White, H. J.; Eyring, H. Text Res J 1945, 15, 295.
5. Zener, C. Elasticity and Anelasticity of Metals; Chicago University Press: Chicago, 1948.
6. Sherby, O. D.; Dorn, J. B. Mech Phys Solids 1958, 6, 145.
7. Wilding, M. A.; Ward, I. M. Polymer 1981, 22, 870.
8. Guiu, F.; Pratt, P. L. Phys Status Solidi B 1964, 6, 111.
9. Sweeney, J.; Ward, I. M. J Mater Sci 1990, 25, 697.
10. Sweeney, J.; Shirataki, H.; Unwin, A. P.; Ward, I. M. J Appl Polym Sci 1999, 74, 3331.
11. Pakula, T.; Trznadel, M. Polymer 1985, 26, 1011.
12. Morshedian, J.; Khonakdar, H. A.; Rasouli, S. Macromol Theory Simul 2005, 14, 428.
13. Bhattacharyya, A.; Tobushi, H. Polym Eng Sci 2000, 40, 2498.
14. Tobushi, H.; Okumura, K.; Hayashi, S.; Ito, N. Mech Mater 2001, 33, 545.
15. Ter Heide, N.; Schlangen, E.; van Breugel, K. Knud Hoejgaard Conference on Advanced Cement-Based Materials; Technical University of Denmark: Copenhagen, 2005.
16. Isaacs, B.; Lark, R. J.; Jefferson, A. D.; Dunn, S. C.; Joseph, C. Mag Concr Res, submitted.
17. Trznadel, M.; Kryszewski, M. Polym Rev 1992, 32, 259.
18. Ward, I. M.; Sweeney, J. An Introduction to the Mechanical Properties of Solid Polymers, 2nd ed.; Wiley: Chichester, England, 2004.
19. Bhushan, B. Mechanics and Reliability of Flexible Magnetic Media, 2nd ed.; Springer-Verlag: New York, 2000.
20. Jog, J. P. Polym Rev 1995, 35, 531.
21. Akhmedov, F. A.; Aikhodzhaev, B. I.; Talipov, G. S. Mech Compos Mater 1968, 4, 626.
22. Simo, J. C.; Hughes, T J. R. Computational Inelasticity; Springer-Verlag: New York, 1998.
23. Sperling, L. H. Introduction to Physical Polymer Science, 4th ed.; Wiley: Hoboken, NJ, 2006.